CrystEngComm

Accepted Manuscript

ROYAL SOCIETY OF CHEMISTRY

www.rsc.org/crystengcomm

Cite this: DOI: 10.1039/c0xx00000x

www.rsc.org/xxxxxx

ARTICLE TYPE

Synthesis of $NaYF_4$: Yb-Tm thin film with strong NIR photon up-conversion photoluminescence using electro-deposition method

Hong Jia,[a] Cheng Xu,[a] Juecheng Wang,[a] Ping Chen,[a] Xiaofeng Liu,*[a] and Jianrong Qiu,*[a b]

Received (in XXX, XXX) Xth XXXXXXXXX 20XX, Accepted Xth XXXXXXXXX 20XX

DOI: 10.1039/b000000x

Rare earth doped fluorides with strong up-conversion (UC) luminescence have attracted growing attention due to their potential applications in photonics and biological areas. However, current techniques to process these fluorides into thin films have not been sufficiently developed. Here, we report for the first time the preparation of $NaYF_4$ thin film doped with Yb^{3+}, Tm^{3+} by electro-deposition and subsequent annealing. The as-deposited thin films were characterized by X-ray diffraction, scanning electron microscopy, thermogravimetry, differential thermal analysis and photoluminescence. Under the excitation by a near infrared laser diode at 980nm, the transparent $NaYF_4$: Yb-Tm thin film exhibits bright visible upconversion luminescence from Tm^{3+} as a result of energy transfer from Yb^{3+}. The results demonstrate that the electro-deposition process provides a facile access to UC fluoride thin films which may have applications in photovoltaic devices.

1 Introduction

Up-conversion (UC) by nanoparticles or glass materials doped with rare-earth (RE) ions, such as Tm^{3+}, Er^{3+}, Ho^{3+}, Nd^{3+}, and Pr^{3+}, have numerous potential applications, including biological labels, photovoltaic degradation, photodynamic therapy, three-dimensional displays, and UC lasers [1-13]. These applications reply on the efficient synthetic procedures that process the UC materials into different forms, such as nanoparticles and thin films. Thin UC films are usually required when they are applied as spectral converters in photovoltaic cells to capture sub-bandgap solar radiation [14-16], multilayer optical storage disks [17], and luminescent screens for optically written displays [18]. Up to now, different UC thin films made from RE activated fluorides [19, 20] or Oxides [21] have been prepared by Sol-gel method or spin-coating process. In Sol-gel process, a post-deposition heat treatment is often applied to reduce the concentration of quencher -OH; while for spin-coating the film quality is usually jeopardized by the poor adhesion between the film and the substrate. In addition to these wet-chemistry route, oxide UC films was also accessed by Pulsed Laser deposition (PLD) [22, 23], which however is a complex technique of relatively high cost.

$NaYF_4$, a host of low phonon energy, is considered to be one of the most efficient UC luminescence host material reported to date [24-26]. However, as it contains fluorine, common methods such as chemical vapor deposition (CVD), PLD, atomic layer deposition (ALD), magnetron sputtering, and spray pyrolysis, are not suitable for the preparation of $NaYF_4$ film. In this work, the $NaYF_4$ thin film doped with Yb^{3+}, Tm^{3+} is prepared by electro-deposition for the first time. For the preparation of $NaYF_4$ thin film, the electro-deposition are simple and cost-efficient and it shows several advantages compared to contemporary process, such as the relatively easy casting of large high-quality sample onto planar or curves surfaces, and excellent adhesion between film and substrate. The $NaYF_4$:Yb-Tm thin films were characterized with X-ray diffraction (XRD), thermogravimetry (TG), differential thermal analysis (DTA) and scanning electron microscopy (SEM). Under the 980 nm laser diode, visible UC emission was observed from the films, and the related mechanisms were discussed.

2 Experimental section

$Y(NO_3)_3$, $Yb(NO_3)_3$ and $Tm(NO_3)_3$ (99.99%) were dissolved in deionized water respectively to get a concentration of 0.1 M for each solutions. These solutions were mixed with a volume ratio of $V[Y(NO_3)_3]$: $V[Yb(NO_3)_3]$: $V[Er(NO_3)_3]$=78: 20: 2, then the same volume of 0.2 M EDTA, 0.5 M sodium ascorbate were added into the mixed solution, forming the stable M-EDTA (M=Y, Yb, Tm) complex. Finally, 0.4 M NH_4F was added to the above solution and the pH of mixture solution was adjusted to 6.6 by 0.1 M NaOH. The solution was used as the precursors for electro-deposition afterwards. All samples were electro-deposited in a conventional three-electrode cell, in which an indium tin oxide coated glass (sheet resistance: 20 Ω/□, purchased from Xiangcity Technology Ltd), a platinum foil and Ag/AgCl/saturated KCl was used as working, counter and reference electrode, respectively. Each sample was deposited at 60 °C for 40 min under the applied potential of 1.2 V (vs Ag/AgCl/saturated KCl). After the deposition, all the samples were cleaned and dried in air at 60 °C for 2 h, and then annealed at various temperatures (300 °C, 400 °C , 500 °C, 560 °C, 680 °C) for 2.5 h in nitrogen.

The crystal structures of all the samples were studied by X-ray diffraction (XRD) with a RIGAKU D/MAX 2550/PC system operated at a step size of 0.02°at a scanning speed of 5°min^{-1} using Cu K_α radiation (λ=1.5406 Å). Thermogravimetry (TG) and Differential thermal analysis (DTA) were carried out on the

TGA7 and DTA7 (Perkin Elmer Co. Ltd., USA) of the Perkin Elmer at a heating rate of 10°C/min. Scanning electron microscope (SEM) images were taken using a Hitachi S-4800 scanning electron microscope. The UV-Vis diffuse reflectance spectra of the films were measured at room temperature on a Hitachi-4100 spectrophotometer. The UC luminescence of the samples was investigated using a FLS920 fluorescence spectrophotometer (Edinburgh Instrument Ltd., U. K.).

3 Results and discussion

3.1 Electrochemical reactions to $NaYF_4$

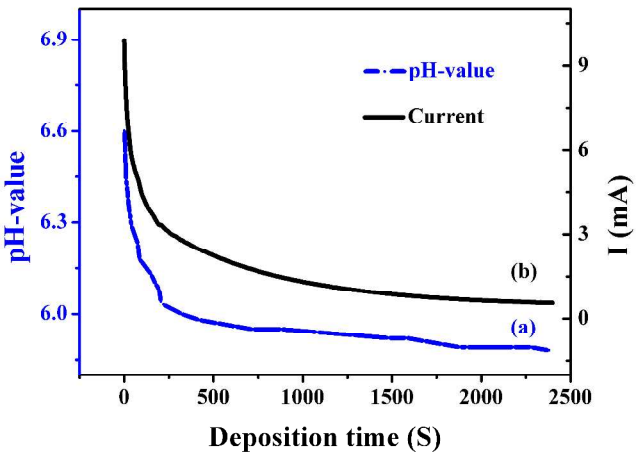

Figure 1. (a) the relation between current and the deposit time, (b) The relation between pH-value of the solution and the deposit time

In electrochemical process, different reduction oxidation reactions are generally involved at different electrodes where the target materials are formed. For the electro-deposition process described here, the formation of $NaYF_4$: Yb-Tm thin film was associated with the following equations:

$$M^{3+} + EDTA \rightarrow M^{3+} - EDTA \quad (1)$$

$$C_6H_7O_6^- \rightarrow C_6H_6O_6 + H^+ + e \quad (2)$$

$$M^{3+} - EDTA + xH^+ \rightarrow H_xEDTA^{x-3} + M^{3+} \quad (3)$$

$$M^{3+} + Na^+ + 4F^- \rightarrow NaMF_4 \downarrow \quad (4)$$

In the equations, the metal ion (M) is the Y, Yb, or Tm, and $C_6H_7O_6^-$ is sodium ascorbate. Under a positive applied voltage, H^+ ions are released by the electrochemical oxidation of ascorbate anion and then reduced the pH of the solution at the surface of the working electrode; afterwards M^{3+} are solvated from the M^{3+}-EDTA complex. It has to be noted here that lanthanide-EDTA complexes are stable only at high pH-values (pH > 5) in the electrolyte solution [27-29]. At the electrode surface, however, as protons are continuously solvated the pH-value of the nearby solution can be much lower than that of the bulk (given in Fig. 1), such that M^{3+}-EDTA complex only dissociate around the electrode, i.e., ITO substrate. In the final step, M^{3+} and Na^+ react with F^- ions near the electrode surface, resulting in the deposition of $NaYF_4$: Yb-Tm particles onto the ITO substrate. Figure 1(a) shows that the deposition current decreases rapidly in the first 250 s and afterwards tends to stabilize, which is in consistence with the change of pH of electrolyte solution (Figure 1b). This result indicates that electro-deposition is closely related with the electron transfer process at the electrode surface. The formation of $NaMF_4$ finally occurs via the solvation of M^{3+} from the M^{3+}-EDTA complex. During further deposition, the growth in thickness of the as-formed $NaMF_4$ film is retarded as fluoride is not conductive, such that the reaction slows down and the current decreases.

3.2 Characterization of the $NaYF_4$ films

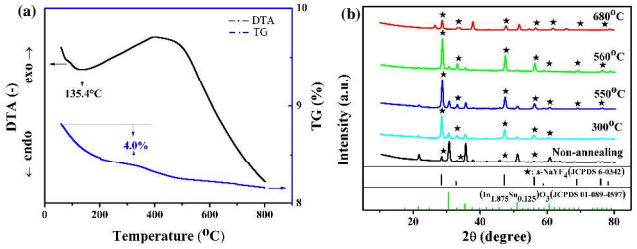

Figure 2. (a) TG and DTA curves of $NaYF_4$: Yb-Tm thin film precursor, (b) X-ray diffractions patterns for samples before and after annealing at different temperature.

Figure 2(a) shows the TG–DTA curves of the as-deposited $NaYF_4$: Yb-Tm thin film during heating from room temperature to 800 °C. An endothermic reaction starting from 94 °C and peaking at 135 °C was observed. The mass loss of 4.0% at 135 °C corresponds to the loss of the absorbed water on the film surface. No obvious mass loss was observed above 250 °C. Figure 2(b) shows the film XRD patterns of $NaYF_4$: 20%Yb-2%Tm films as a function of annealing temperature from 300 °C to 680 °C. In the as-prepared film, the XRD can be indexed to the pure cubic phase of $NaYF_4$ (JCPDS card No. 06-0342), and no other phase can be identified after annealing at 300 °C, 550 °C, 560 °C and 680 °C. The crystalline size as calculated from Scherrer equation increases from 152 nm (300 °C) to 188 nm (560 °C) due to temperature driven crystal growth for the fluoride particles. However, for the sample annealed at 680 °C diffraction intensities become smaller suggesting that the crystals of the $NaYF_4$ tends to collapse. This result may relate with the chemical instabilities of fluoride on the ITO substrate at high temperature, or possibly due to the sublimation of the metal fluoride.

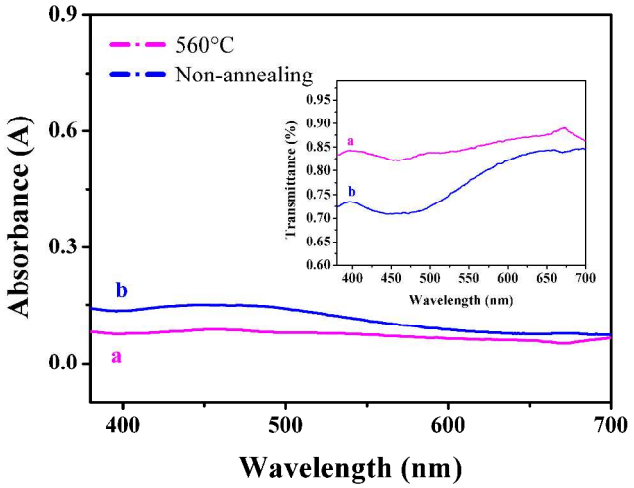

Figure 3. (a) The absorbance of the transparent film after annealing at 560 °C for 2.5 h (the insert picture a is the transmittance of the annealed film), (b) the absorbance of the as-deposited transparent film (the insert picture b is the transmittance of as-deposited transparent film)

The thin films deposited on ITO before and after annealing still exhibits satisfactory transparency. Figure 3 presents the absorption curves of the electro-deposited fluoride films. Compared with the annealed samples, the as-deposited film (without annealing) shows better transparency especially at shorter wavelength. This difference in transparency reflects the effect of annealing on the microstructures of the thin films. Due to increased scattering loss by the larger particles, the annealed films become slightly translucent, as can be seen from the digital pictures.

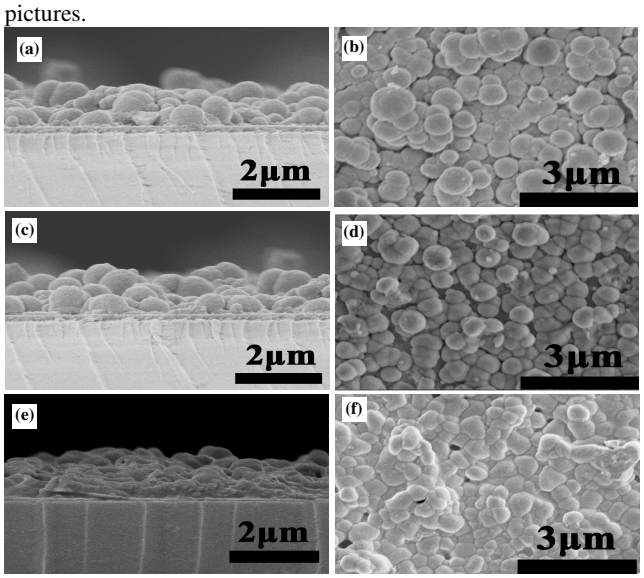

Figure 4. SEM of transparent thin films before and after annealing: (a) SEM image of a cross-section of the as-deposited transparent film, (b) SEM image of the as-deposited film, (c) SEM image of a cross-section obtain from a film after annealing at 560 ^{o}C for 2.5 h, (d) SEM image of the film after annealing at 560 ^{o}C for 2.5 h. (e) SEM image of a cross-section obtain from a transparent film after annealing at 680 ^{o}C for 2.5 h, (f) SEM image of the film after annealing at 680 ^{o}C for 2.5 h.

The SEM images of the thin films before and after annealing are shown in Figure 4. From the cross- section image given in Figure 3a, the film before annealing has a thickness of around 900 nm, and it consists of densely packed spherical particles of the size around 500±200 nm. Fig. 4c and 4d is the cross-section and surface SEM images of the $NaYF_4$: 20%Yb-2%Tm film after annealing at 560 ^{o}C for 2.5 h. The film shows similar surface morphologies with regular orientation and ordered array of spheres. In addition, the thickness of the film is not changed with the increase in annealing temperature, while the surfaces of particles in the thin film become smooth as a result of crystal growth. At high temperature (680 ^{o}C), the $NaYF_4$ particles seem unstable. As can be seen from Figure 4e and 3f, the spherical particles are all fused together and the initial morphology completely collapsed, which is also reflected by the weakening of the XRD intensity as shown in Figure 2b. This structural change may arise from the reaction of the deposited with the substrate glass or due to the sublimation of fluoride. The exact mechanism remains to be examined in more detail.

3.3 Up-Conversion Photoluminescence Properties

With the excitation by a 980 nm LD, UC emission was observed from the film ($NaYF_4$: 20%Yb-2%Tm) annealed at different temperature for 2.5 h (Figure 5a). Three UC emission bands are clearly resolved. Blue emission bands observed from 486 nm are associated with the $^1G_4 \rightarrow {}^3H_6$ transitions, while red bands peaking at 655 nm are associated with the $^1G_4 \rightarrow {}^3F_4$ transition. The strongest and sharp peak at 797 nm matches with the $^3H_4 \rightarrow {}^3H_6$ transitions of the Tm^{3+}. The difference between the emission intensity is because $^3H_4$ state excited process is populated via two excitation photons, which has higher transition probability than the three-photon excited state $^1G_4$ (denoted in figure 5c and 5d). Although the UC emission at 797 nm is invisible to naked eye, a brightly visible blue UC emission can be clearly observed by naked eye.

The films without annealing or annealing at different temperatures show similar UC emission bands. The UC emission intensity of the films increases with the annealing temperature from 300 to 560 ^{o}C, and then decreases at higher annealing temperature. The increase in UC can be obviously associated to the improvement in crystallinity of the films at high annealing temperatures. However, at 680 ^{o}C the particles in the film collapse possibly due to sublimation or reaction with the substrate, as found by the above structural analysis, as a result the UC emission was reduced.

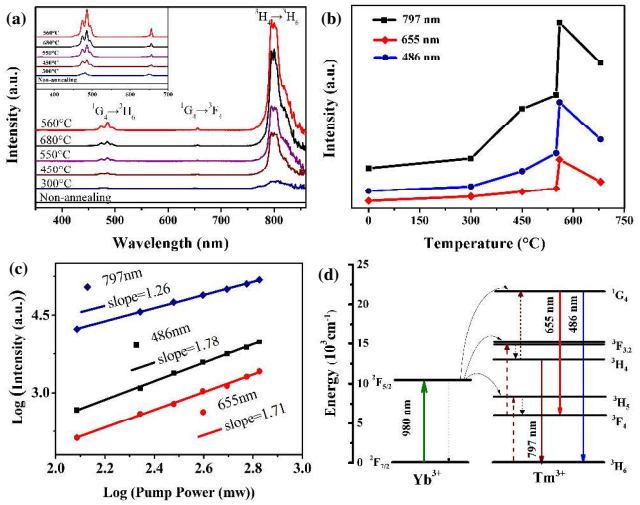

Figure 5. (a) and (b) UC emission spectra from the $NaYF_4$: Yb-Tm thin films before and after annealing at different temperature for 2.5 h, (c) Power dependence of UC intensity of the $NaYF_4$: Yb-Tm thin film doped with 20%Yb, 2%Tm measured at 486, 655 and 797 nm, respectively, (d) Proposed energy transfer mechanisms under 980 nm LD excitation in the $NaYF_4$: 20%Yb-2%Tm thin film.

It is well known that the dependence of UC intensity on pump power is essential for identification of the UC mechanism. For any UC process, the relationship between the intensity (I) and the pump power (p) is approximately expressed by the following equation:

$$I \propto P^{n} \quad (5)$$

Where the number of pumping photons (n) required to exciting ions from the ground state to the emitting state can be determined from the slope of the photoluminescence (PL) versus the laser excitation power in a log-log plot. The dependence of UC luminescence intensity of the $NaYF_4$: 20%Yb-2%Tm thin film upon pump power is shown in Figure 5c. The double logarithmic plot of the measured intensity of emission at 486 nm, 655 nm and 797 nm versus the pump power yields three straight lines with

slope of 2.8, 2.2, and 1.5, respectively, illustrating the 797 nm emission is generated by two excitation photons while the 655 nm and 486 nm emission with three-photons excitation. The energy level diagrams of the Yb^{3+}-Tm^{3+} ions as well as the energy transitions mechanism are shown in Figure 5d. Since Tm^{3+} ions have no excited energy level at round 980 nm, so the corresponding photons are absorbed exclusively by Yb^{3+} ions, which afterwards transfer this pump energy to nearby Tm^{3+} ions. Tm^{3+} ion was then promoted from its the ground state ($^3H_6$) to the $^3H_5$ state with the excessive energy dissipated by phonons. Subsequently, the Tm^{3+} ions in the $^3H_5$ state relaxes nonradiatively to the lower state of the $^3F_4$, and then populates to the $^3F_{2,3}$ state by a second energy transition from the Yb^{3+} ion to the Tm^{3+} ion. However, the Tm^{3+} ion in the $^3F_{2,3}$ state is unstable, it relaxes to the $^3H_4$ state through the efficient non-radiative transition. Lastly, the Tm^{3+} ion gives strong UC emission with the peak at 979 nm from the $^3H_4$ state to the $^3H_6$ state. The Tm^{3+} ions in the $^3H_4$ state can also be excited to the $^1G_4$ state by further energy transfer from the Yb^{3+} ions after absorbing another photons, and then decay radiatively to the $^3F_4$ and $^3H_6$ state generating red and blue UC emissions around at 655 nm and 486 nm, respectively [30].

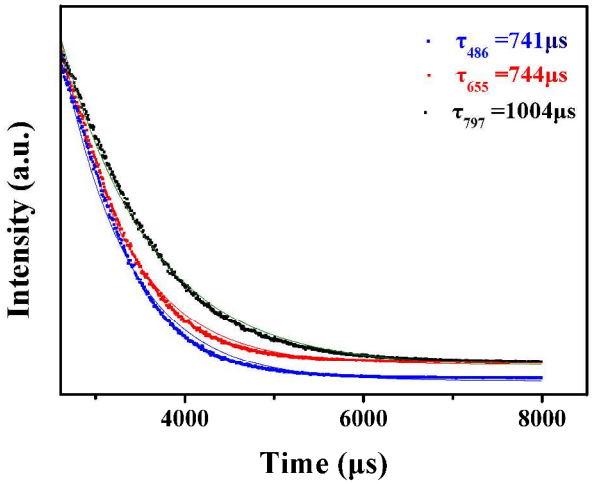

Figure 6. Time evolution of blue (486 nm), red (655 nm) and near-infrared emission (797 nm) UC luminescence, under pulsed 980nnm excitation, from a thin film of the $NaYF_4$: 20%Yb-2%Tm annealing at 560 °C for 2.5 h.

Figure 6 displays the time dependence of blue (Tm^{3+}: $^1G_4 \rightarrow {}^3H_6$) , red ($Tm^{3+}$: $^1G_4 \rightarrow {}^3F_4$) and near-infrared emission (Tm^{3+}: $^3H_4 \rightarrow {}^3H_6$) UC luminescence in the $NaYF_4$: 20%Yb-2%Tm thin film after cease of the excitation at 980 nm. Blue and red UC emission which are originate from the same $^1G_4$ state (see Figure 4d) have similar lifetimes of around 740 μs; in comparison the intermediate $^3H_4$ state has much longer decay times over 1 ms. It is because the rise components in the measurement should be determined through the lifetime of the latter state, however, the decay time of the UC luminescence kinetics are determined by the intermediate state of $^3H_4$ [31].

4 Conclusions

Thin films of $NaYF_4$: 20%Yb-2%Tm is prepared by electro-deposition followed by annealing at high temperatures. The deposited films is transparent, and show three UC emissions at 797 nm, 655 nm and 486nm due to the transitions $^3H_4 \rightarrow {}^3H_6$, $^1G_4 \rightarrow {}^3F_4$ and $^1G_4 \rightarrow {}^3H_6$ of Tm^{3+}. The UC emission intensity of the $NaYF_4$: 20%Yb-2%Tm thin films increases with the annealing temperature and the film annealed at 560 °C for 2.5 h in nitrogen exhibits strongest UC emission. Excited state absorption and energy transfer processes were proposed as the possible mechanisms based on the energy diagrams of Yb^{3+}-Tm^{3+} ion pair. The result of the present study may pave the way towards the application of electro-deposited fluoride UC films for as spectral converter in solar cells.

Acknowledgements

This work was financially supported by the National Natural Science Foundation of China (Grants 51132004, 51072054, and 51102209) and the National Basic Research Program of China (2011CB808100).

Notes and references

[a] *State Key Laboratory of Silicon Materials, Department of Materials Science and Engineering, Zhejiang University, Hangzhou 310027, China*
[b] *State Key Laboratory of Luminescent Materials and Devices, South China University of Technology, Guangzhou 510640, China*

1 Downing, E.; Hesselink, L.; Ralston, J.; Macfarlane, R. A Three-Color, Solid-State, Three-Dimensional Display. *Science* 1996, *273*, 1185-1189.
2 Bass, M.; Rapaport, A.; Jennsen, H. Dispersed Crystallite Up-Conversion Displays. *U. S. Pat.*, **2003,** *6,* 654161.
3 Shalav, A.; Richards, B. S.; Green, M. A. Luminescent Layers for Enhanced Silicon Solar Cell Performance: Up-Conversion. *Sol. Energ. Mat. Sol. C.* 2007, *91*, 829-842.
4 Wild, J.; Rath, J. K.; Meijerink, A.; van Sark, W. G. J. H. M.; Schropp, R. E. I. Enhanced Near-Infrared Response of a-Si: H Solar Cells with b-$NaYF_4$: Yb^{3+} (18%), Er^{3+} (2%) Upconversion Phosphors. *Sol. Energ. Mat. Sol. C.* **2010**, *94*, 2395-2398.
5 Wang, H-Q, Batentschuk, M.; Ovet, A.; Pinna, L.; Brabec, C. J. Rare-Earth Ion Doped Up-Conversion Materials for Photovoltaic Applications. *Adv. Mater.* **2011,** *23*, 2675-2680.
6 Nyk, M.; Kumar, R.; Ohulchanskyy, T. Y.; Bergey, E. J.; Prasad, P. N. High Contrast in Vitro and in Vivo Photoluminescence Bioimaging Using Near Infrared to Near Infrared Up-Conversion in Tm^{3+} and Yb^{3+} Doped Fluoride Nanophosphors. *Nano Lett.* **2008**, *8*, 3834-3838.
7 Zou W. Q.; Visser, C.; Maduro, J. A.; Pshenichnikov, M. S.; Hummelen, J. C. Broadband Dye-Sensitized Upconversion of Near-Infrared Light. *Nat. Photonics.* **2012**, *6*, 560-564.\
8 Xie, X. J.; Liu X. G.; Upconversion goes broadband. *Nat. Mater.* **2012**, *11*, 842-843.
9 Trupke, T.; Green, M. A.; Würfel, P. Improving Solar Cell Efficiencies by Up-Conversion of Sub-Band-Gap Light. *J. Appl. Phys.* **2002**, *92*, 4117-4122.
10 Ye, O. L.; Yang, X. X.; Li, C. L.; Li, Z. Q. Synthesis of UV/NIR photocatalysts by coating TiO_2 shell on peanut-like YF_3:Yb,Tm upconversion nanocrystals. *Mater. Lett.* 2013, *106*, 238-241.
11 Li, C. X.; Lin, J. Rare earth fluoride nano-microcrystals: synthesis, surface modification and application *J. Mater. Chem.* **2010**, *20*, 6831-6847.
12 Ma, P. A.; Xiao, H. H.; Li, X. X.; Li, C. X.; Dai, Y. L.; Cheng, Z. Y.; Jing, X. B and Lin, J. Rational Design of Multifunctional Upconversion Nanocrystals/Polymer Nanocomposites for Cisplatin (IV) Delivery and Biomedical Imaging. *Adv. Mater.* **2013**, *25*, 4898-4905.
13 Gu, Z. J.; Yan, L.; Tian, G.; Li, S. J.; Chai, Z. F. and Zhao, Y. L. Recent Advances in Design and Fabrication of Upconversion

Nanoparticles and Their Safe Theranostic Applications. *Adv. Mater.* **2013**, *25*, 3758–3779.

14 Shalav, A. ; Richards, B. S.; Trupke, T.; Krämer, K. W.; Güdel, H. U.; Application of $NaYF_4$: Er^{3+} Up-converting Phosphors for Enhanced Near-infrared Silicon Solar Cell Response. *Appl. Phys. Lett.* **2005**, *86*, 013505-3.

15 Richards, B. S.; Shalav, A. The Role of Polymers in the Luminescence Conversion of Sunlight for Enhanced Solar Cell Performance. *Synth. Met.* **2005**, *154*, 61-64.

16 Su, L. T.; Karuturi, S. K.; Luo, J. S.; Liu, L. J.; Liu, X. F.; Guo, J.; Sum, T. C.; Deng, R. R.; Fan, H. J.; Liu, X. G.; Tok, L. Y. Photon Upconversion in Hetwro-nanostructured Photoanodes for Enhanced Near-Infrered Lingt Harvestiong. *Adv. Mater.* **2013**, *25*, 1603-1607.

17 Ho, H. P.; Wong, W. W.; Wu, S. Y. Multilayer Optical Storage Disk Based on the Frequency Up-conversion Effect from Rare-earth Ions. *Opt. Eng.* **2003**, *42*, 2349-2353.

18 Wang, Q. H.; Bass, M. Photo-luminescent Screens for Optically Written Displays Based on Upconversion of Near Infrared Light. *Electron. Lett.* **2004**, *40*, 987-988.

19 Sivakumar, S.; vanVeggel, F. C. J.M.; May, P. S. J. Near-Infrared (NIR) to Red and Green Up-Conversion Emission from Silica Sol–Gel Thin Films Made with $La_{0.45}Yb_{0.50}Er_{0.05}F_3$ Nanoparticles, Hetero-Looping-Enhanced Energy Transfer (Hetero-LEET): A New Up-Conversion Process. *J. Am. Chem. Soc.* **2007,** *129*, 620-625.

20 Sivakumar, S.; vanVeggel, F. C. J.M.; Raudedsepp, M. J. Bright White Light through Up-Conversion of a Single NIR Source from Sol–Gel-Derived Thin Film Made with Ln^{3+}-Doped LaF_3 Nanoparticles. *J. Am. Chem. Soc.* **2005,** *127*, 12464-12465.

21 Que, W.; Zhou, Y. L.; Pita, K.; Chan, Y. C.; Kam, C. H. Luminescence Properties from Erbium Oxide Nanocrystals Dispersed in Titania/organically Modified Silane Composite Sol–gel thin films. *Appl. Phys. A: Mater. Sci. Process.* **2001,** *73*, 209-213.

22 Qin, G.; Qin, W.; Wu, C.; Wu, C.; Huang , S.; Zhang, J.; Zhao,D.; Liu, H. J. Enhancement of Ultraviolet Upconversion in Yb^{3+} and Tm^{3+} Codoped Amorphouss Fluoride Film Prepared by Pulsed Laser Deposition. *Appl. Phys.* **2003,** *93*, 4328-4330.

23 Bubb, D. M.; Cohen, D.; Qadri, S. B. Infrared-to-visible upconversion in thin films of LaEr- $-(MoO_4)_3$. *Appl. Phys. Lett.* **2005**, *87*, 131909-3.

24 Dong, H.; Sun, L. D.; Yan, C. H.; Basic understanding of the lanthanide related upconversion emissions. *Nanoscale*. **2013**, *5*, 5703-5714.

25 Wang, L.; Li, Y. D. $Na(Y_{1.5}Na_{0.5})F_6$ Single-Crystal Nanorods as Multicolor Luminescent Materials**.** *Nano. Lett.* **2006**, *6*, 1645-1649.

26 Zhou, J.; Liu, Z.; Li, F.. Upconversion Nanophosphors for Small-animal imaging.*Chem. Soc. Rev.* **2012**, *41*, 1323–1349.

27 Wheelwright, E. J.; Spedding, F. H.; Schwarzenbach, G. The Stability of the Rare Earth Complexes with Ethylenediaminetetraacetic Acid. *J. Am. Chem. Soc.*, **1953**, *75*, 4196–4201

28 Moeller, T.; Martin, D. F.; Thompson, L. C.; Ferrus, R.; Feistel, G. R.; Randall, W. J. The Coordination Chemistry of Yttrium and the Rare Earth Metal Ions. *Chem. Rev.* **1965**, *65*, 1–50.

29 Cam, T.; Irez, G.; Aydin, R. Determination of Stability Constants of Mixed Ligand Complexes of the Lanthanum(III)Ion and Identification of Structures. *J. Chem. Eng. Data*. **2011**, *56*, 1813–1820

30 Chen, G. Y.; Ohulchanskyy, T. Y.; Kumar, R.; Ågren, H.; Prasad, P. N. High-Quality Sodium Rare-Earth Fluoride Nanocrystals: Controlled Synthesis and Optical Properties. *ACS Nano*. **2010**, *4*, 3163–3168.

31 Zhou, J. J.; Shirahata, N.; Sun, H. T.; GHosh, B.; Ogawara, M.; Teng, Y.; Zhou, S. F.; Chu, R. G. S.; Fujii, M.; Qiu, J. R.Efficient Dual-Modal NIR-to-NIR Emission of Rare Earth Ions Co-doped Nanocrystals for Biological Fluorescence Imaging. *J. Phys. Chem. Lett.* **2013**, *4*, 402-408.

Color Graphic

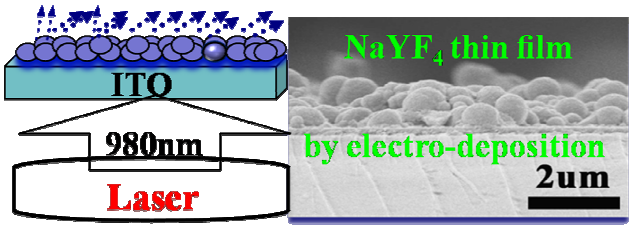

The $NaYF_4$: 20%Yb-2%Tm thin film prepared by electro-deposition perform the strong UC photoluminescence.

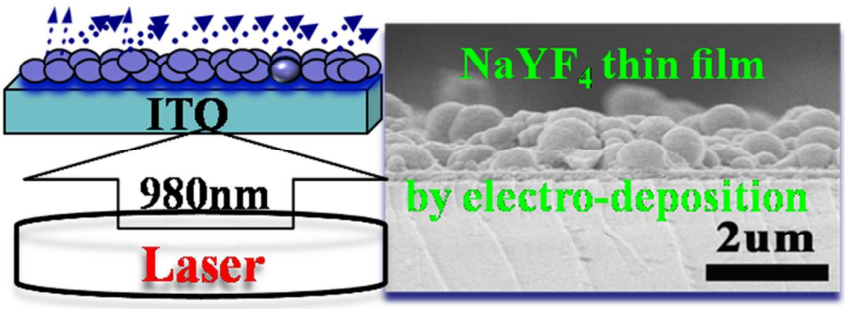

The $NaYF_4$: 20%Yb-2%Tm thin film prepared by electro-deposition perform the strong UC photoluminescence